

Article

Numerical Computation of Hydrodynamic Characteristics of an Automated Hand-Washing System

Thanh-Long Le ^{1,2,*} , Thi-Hong-Nhi Vuong ^{2,3}  and Tran-Hanh Phung ^{1,2}

¹ Faculty of Mechanical Engineering, Ho Chi Minh City University of Technology (HCMUT), 268 Ly Thuong Kiet Street, District 10, Ho Chi Minh City 700000, Vietnam; hanh.phungcokhi.19_3@hcmut.edu.vn

² Vietnam National University Ho Chi Minh City, Linh Trung Ward, Ho Chi Minh City 700000, Vietnam; vthnhi@hcmut.edu.vn

³ Faculty of Transportation Engineering, Ho Chi Minh City University of Technology (HCMUT), 268 Ly Thuong Kiet Street, District 10, Ho Chi Minh City 700000, Vietnam

* Correspondence: tllong@hcmut.edu.vn

Abstract: The aim of this study is to develop a physical model and investigate the bactericidal effect of an automated hand-washing system through numerical computation, which is essential in areas affected by COVID-19 to ensure safety and limit the spread of the pandemic. The computational fluid dynamics approach is used to study the movement of the solution inside the hand-washing chamber. The finite element method with the $k-\epsilon$ model is applied to solve the incompressible Navier–Stokes equations. The numerical results provide insights into the solution’s hydrodynamic values, streamlines, and density in the two cases of with a hand and without a hand. The pressure and mean velocity of the fluid in the hand-washing chamber increases when the inlet flow rates increase. When the hand-washing chamber operates, it creates whirlpools around the hands, which remove bacteria. In addition, the liquid inlet flow affects the pressure in the hand-washing chamber. The ability to predict the hydraulic and cleaning performance efficiencies of the hand-washing chamber is crucial for evaluating its operability and improving its design in the future.

Keywords: numerical computation; computational fluid dynamics; hydrodynamic values; hand-washing chamber



Citation: Le, T.-L.; Vuong, T.-H.-N.; Phung, T.-H. Numerical

Computation of Hydrodynamic Characteristics of an Automated Hand-Washing System. *Computation* **2023**, *11*, 167. <https://doi.org/10.3390/computation11090167>

Academic Editor: Sergey A. Karabasov

Received: 15 July 2023

Revised: 18 August 2023

Accepted: 21 August 2023

Published: 22 August 2023



Copyright: © 2023 by the authors. Licensee MDPI, Basel, Switzerland. This article is an open access article distributed under the terms and conditions of the Creative Commons Attribution (CC BY) license (<https://creativecommons.org/licenses/by/4.0/>).

1. Introduction

During 2020, the SARS-CoV-2 virus rapidly spread across the globe, causing significant damage to economies and claiming many lives. Even now, the virus remains unpredictable and has resurfaced in some countries with new strains such as Omicron and its sub-variants. This lack of information about the virus has created a void that is driving innovation in many fields. Since ancient times, people have faced health problems related to viruses. Over time, people have invented many different ways to prevent those pathogens. Scientists have studied the properties of the coronavirus, thereby creating a vaccine against COVID-19 [1]. According to WHO, people did not stop working to prevent smallpox despite the material constraints caused by the war [2]. As a result, hand-washing with soap has emerged as an example of rapid innovation to combat the COVID-19 global pandemic.

Numerous scientific studies have focused on researching hand-washing machines. One such study by Allegranzi et al. [3] examined the factors that impact hand hygiene compliance in healthcare and the effects of promoting hand hygiene on the rates of cross-transmission and associated pathogen infections. The hands of healthcare workers are often the primary mode of transmission for healthcare-associated pathogens between patients and within the healthcare environment. To prevent the spread of antimicrobial resistance and reduce healthcare-associated infections (HCAIs), hand hygiene is considered the most effective measure. However, despite this knowledge, healthcare worker adherence

to optimal hand hygiene practices remains low in most healthcare settings. Thorough hand washing is a simple yet effective way to prevent the spread of illnesses and diseases. However, compliance with proper hand-washing techniques remains a significant issue globally. Conover et al. [4] conducted a study that summarized the factors affecting hand washing. Hand sanitizers can be antimicrobial or non-antimicrobial in terms of the content of important substances used in the solution. The time taken to wash hands must be suitable for hand washing to be effective and to optimize operating costs. In addition, the paper also presented an evaluation of the effectiveness of hand washing using two main methods: hand inoculation and the removal of microorganisms from hands. Recently, Kukkala et al. [5] devised a standalone device that can automatically wash a user's hands without the need for the user to touch anything during or after the process, demonstrating equally good decontamination. Users can place their hands in the machine and allow it to perform various cycles, including wash, soap, scrub, and dry cycles, resulting in clean hands. Jolan et al. [6] conducted a study on the effectiveness of multi-station automatic hand-washing systems, which provide complete and hygienic hand-washing activities with soap and water through multiple stations that operate independently of each other. These systems meet the WHO hand-washing duration standard and accommodate the WHO hand-washing technique, making them an effective solution for promoting proper hand hygiene.

Computational fluid dynamics (CFD) is known as an important technology for the study of the hydro-aerodynamic characteristics of fluid motion, and has been applied to a microchannel, sterilization chamber, torpedo-shaped underwater glider, centrifugal blower, an infection isolation room, etc. [7–14]. Le et al. [7–10] investigated the thermocapillary migration of the fluid flows in a microchannel. The numerical results showed that the heat and mass transfer problems strongly affect the motion behavior of fluids in a microchannel. Feurhuber et al. [15] utilized CFD simulation to measure the temperature and pressure in sterilizers. In addition, the estimation of non-condensable gases (NCGs) in stream sterilizers has an important role in calculating the real volume fraction of NCGs. The volume fractions of NCGs within steam sterilizers, according to many indexes such as fluid flow, temperature, and heat transfer, are separated in time and space. Lewinski et al. [16] studied the effectiveness of iron oxide nanoparticles to remove the bacteria from human skin. The research indicated $\gamma - \text{Fe}_2\text{O}_3$, ZnO nanoparticles have a remarkable ability to remove pathogens attached to the surface of human skin. Vuai et al. [17] investigated the disinfection effectiveness of hand sanitizer products on the market to mitigate the COVID-19 outbreak. The research indicated that there is a need to develop cleaning and disinfecting products and processes that are more effective against present and future pathogens. Huang et al. [18] demonstrated the effect of parameters on the hydrodynamics of a high-pressure water-jet nozzle. The results indicated the impact of the sprinkler characteristics on the performance and behavior of the nozzles. CFD analysis has rarely been used to analyze the hydrodynamic characteristics of the flow in hand-washing machines. Nonetheless, it is an interesting approach that could improve the cleaning performance of these machines.

The purpose of this paper is to develop a parametric representation of an automated hand-washing system and enhance its hydrodynamic performance using a feasible method. The proposed approach involves representing the system's profile using velocity values at the inlet and pressure values at the outlet, which are then optimized to improve the system's hydrodynamic efficiency and cleaning performance. To evaluate the profile's performance at specific sample points in the design space, CFD analysis is conducted.

2. Methodology

2.1. Physical Model

In this study, a physical model of the hand-washing chamber was designed to represent all the important features of this chamber in real life. The model is guaranteed to be widely used and suitable for most Vietnamese people with an average arm length of 0.65 m or

more. For these needs, this rotating chamber has a diameter of 0.2 m and a height of 0.32 m (the part of the hand to be washed is half the average arm length). This hand-washing rotary chamber has entry and exit points, a chemical tank, and a spray mechanism system. According to the size of the chamber, the liquid flow is calculated to ensure that the disinfectant liquid is sprayed all over the hand after 20 s.

$$q = \frac{\delta V}{\delta t} = \frac{1.6}{20} = 0.01 \text{ m}^3/\text{s} \quad (1)$$

The CleanTech Automated Hand-Washing System (CTAHS) ensures complete control of hand hygiene. The system has a compact design with a turnstile that automatically opens at the end of each 12 s wash and rinse cycle, and uses 75% less soap and water than manual washes. It also removes 99.98% of dangerous pathogens from bare skin and gloved hands. The CleanTech Automated Hand-Washing System is designed for high-use areas and can wash the hands of up to 4–5 users per minute. It is ideal for environments such as food processing areas, clean rooms, and pharmaceutical manufacturers where effective hand hygiene is critical. This study used a combination of computational fluid dynamics (CFD) and the Fluent module of Ansys Workbench to obtain predictions about the behavior and movement of disinfection solution in this hand-washing rotating chamber. In this model, the results were surveyed for 20 s. Figure 1 shows the 3D model of the hand-washing machine and the vortex chamber in which hands are washed. The 3D model was designed using SOLIDWORKS software. Within the scope of this article, we only introduce the model of the redesigned hand-washing machine based on CTAHS; in this article, we do not provide a detailed discussion of the mechanical design and control issues.

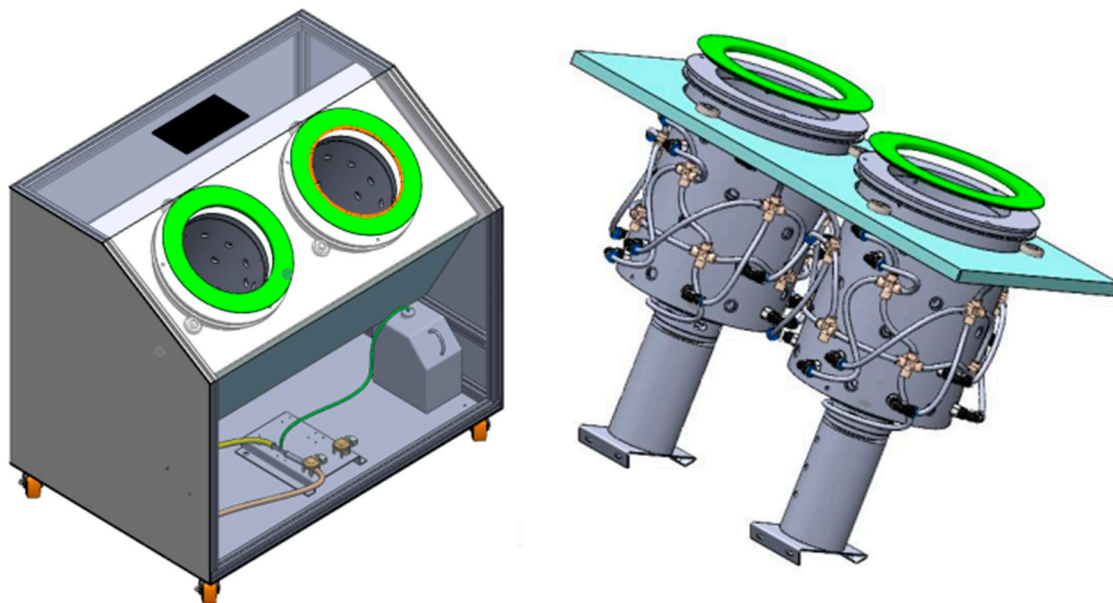


Figure 1. Machine 3D hand-washing model and vortex chamber in which hands are washed.

In this study, the model was built based on the hand-washing rotating chamber in real life. However, the main purpose of this study was to observe the distribution of the solution inside the chamber, which means some solid parts of this chamber are not included. In Figure 2, a model of the hand-washing chamber is presented with two forms, i.e., with and without a human hand. Position 1 is the inlet, position 2 is the outlet, and the fluid used is water. Water is sprayed from the inlets at a speed of 5 m/s. The fluid moves in rotation in the chamber and then exits the chamber via the outlet position. The model has the inputs arranged in 3 different ways. The drainage part is arranged below the chamber rotation, ensuring effective water removal. The holes are clustered together, optimizing the water

flow and distribution. To further enhance effective water drainage, each nozzle cluster is designed with equal rotation angles.

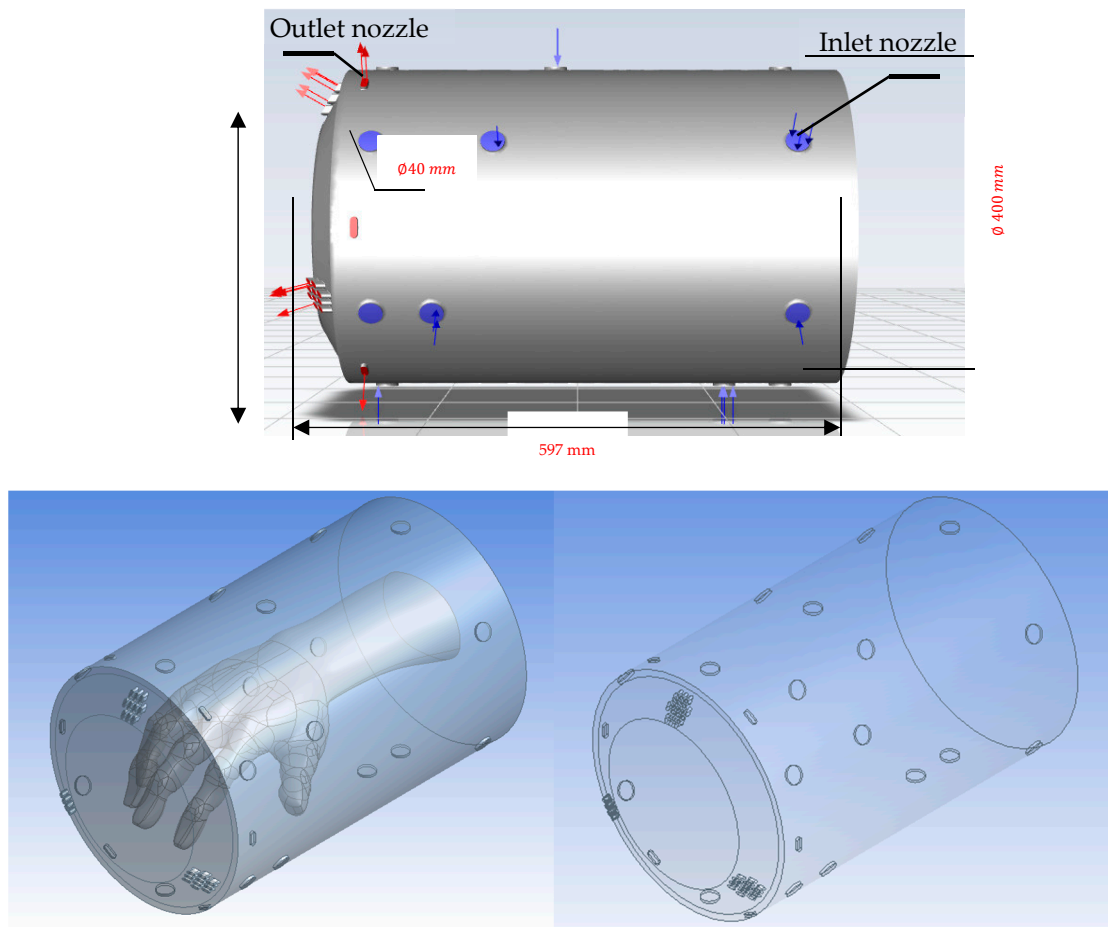


Figure 2. A model of the hand-washing chamber.

In the design of the rotating washing chamber, the solution is sprayed through nozzles installed in the chamber. For the purpose of obtaining simulation results in this study, the Navier–Stokes equations, conservation of mass, kinetic energy, and some related equations are used to analyze the flow of fluids in three dimensions.

Navier–Stokes equation:

$$\rho \left(\frac{\partial \mathbf{u}}{\partial t} + \mathbf{u} \cdot \nabla \mathbf{u} \right) = -\nabla p + \nabla \cdot \mathbb{T} + \mathbf{F} \tag{2}$$

The conservation of mass:

$$\frac{\partial \rho}{\partial t} + \nabla \cdot (\rho \cdot \mathbf{u}) = 0 \tag{3}$$

where:

ρ is the density (SI unit: kg/m^3)

\mathbf{u} is the velocity vector (SI unit: m/s)

p is the pressure (SI unit: Pa)

\mathbf{F} is the volume force vector (SI unit: N/m^3).

In this study, the sterilization chamber was analyzed using the achievable $k-\epsilon$ module. Shin et al. [19] investigated a new $k-\epsilon$ eddy viscosity model for high Reynolds number turbulent flows. The $k-\epsilon$ eddy viscosity formulation describes realizability and includes the effects of mean rotation homogeneous shear flows; boundary-free shear flows; channel and flat boundary layer flows, with and without a pressure gradient; and backward-facing

step flows. This module is known for computing turbulent flow by evaluating the kinetic energy (k) and the turbulent dissipation (ϵ). The achievable k - ϵ modulus is widely used in turbulence models in research or industrial applications because it provides better results and reduces the number of computations in turbulent flow [20].

The kinetic energy equation (k):

$$\frac{\partial}{\partial t}(\rho k) + \frac{\partial}{\partial x_j}(\rho k u_j) = \frac{\partial}{\partial x_j} \left[\left(\mu + \frac{\mu_t}{\sigma_k} \right) \frac{\partial k}{\partial x_j} \right] + G_k + G_b - \rho \epsilon - Y_M + S_k \quad (4)$$

The turbulent dissipation equation (ϵ):

$$\frac{\partial}{\partial t}(\rho \epsilon) + \frac{\partial}{\partial x_j}(\rho \epsilon u_j) = \frac{\partial}{\partial x_j} \left[\left(\mu + \frac{\mu_t}{\sigma_\epsilon} \right) \frac{\partial \epsilon}{\partial x_j} \right] + G_k C_{1\epsilon} \frac{\epsilon}{k} - \rho C_{2\epsilon} \frac{\epsilon^2}{k} + C_{1\epsilon} \frac{\epsilon}{k} C_{3\epsilon} G_b + S_\epsilon \quad (5)$$

where:

G_k : turbulent kinetic energy due to the mean velocity

G_b : turbulent kinetic energy due to buoyancy

$C_{1\epsilon} = 1.44$

$C_{2\epsilon} = 1.92$

$C_\mu = 0.09$

$S = \sqrt{2S_{ij}S_{ij}}$

u_j is the velocity component in the corresponding direction

μ_t is eddy viscosity, $\mu_t = \rho C_\mu \frac{k^2}{\epsilon}$

$\sigma_k = 1$ turbulent Prandtl numbers for k

$\sigma_\epsilon = 1.3$ turbulent Prandtl numbers for ϵ

Y_M : the overall dissipation rate

S_ϵ, S_k : user-defined source terms.

Bernoulli's equation:

$$p + \frac{1}{2}\rho V^2 + \rho gh = \text{constant}$$

where:

p is the pressure (SI unit: Pa)

ρ is the density (SI unit: kg/m³)

V is the velocity

h is elevation

g is the gravitational acceleration (SI unit: m/s²).

2.2. Numerical Methods

Due to the development of computer technology, CFD is now widely used to estimate the motion and hydrodynamic properties of objects in a fluid environment. Most studies are based on Navier–Stokes equations and initial boundary conditions to analyze and obtain velocity values, pressure distribution, kinetic energy, etc. To analyze various fluid flows, we can use continuity equations, momentum equations, and energy equations. Since it is too difficult to calculate all the hydrodynamic values when analytically solving these equations, CFD was applied to derive the results. However, estimating values via CFD helps to improve accuracy and reduce computation time. Feurhuber et al. [15] applied this approach to much of his research. The CFD model of the steam sterilizer was developed to simulate the inactivation of microorganisms at each position within the steam sterilizer [21]. The results indicated that the simulated temperatures are in very good accordance with the measured data. The CFD approach is applied to develop all of the phenomena that occur inside the steam sterilizer, and particularly inside the hollow load PCD tests [22]. Ref. [23] examined the reality of hand washing in some low-income countries around the world, where people have difficulty accessing hand-washing chambers. All of the research

presented below shows that the use of CFD to predict the hydrodynamic properties and motion of liquid flow in a sterilization chamber is suitable.

2.3. Boundary Layer

The mesh is created to suitably model the boundary layer [24] and the layer thickness near the profile person's hand can be calculated as:

$$\Delta y = L\Delta y^+ \sqrt{80} Re^{-\frac{13}{14}} \quad (6)$$

where Re is the Reynolds number defined as VL/γ , where V is the velocity liquid, γ is the coefficient of kinematic viscosity, L is the length of the hand in the chamber, and $20 \leq \Delta y^+ \leq 200$. The thickness of the boundary layer and the first layer close to the hand is approximately 5 mm.

Turbulence was modeled with a turbulence intensity of 5%. The steam quality at the inlet is indicated in Equation (7).

$$x = \frac{m_{steam}}{m_{steam} + m_{water}} \quad (7)$$

where:

m_{steam} : stand for mass of the steam.

m_{water} : the mass of the water.

2.4. Boundary Conditions for Rotatory Simulations

Boundary conditions were applied to simulate hydrodynamic values, streamlines, and density in the two cases of with a hand and without a hand, including a velocity inlet, a pressure outlet with zero relative pressure, a moving wall, and no slip wall. In this study, the rotational speed of the hand-washing chamber was set to 40 rad/s.

2.5. Mesh Generation

In Figure 3, a typical mesh is used in the computational domain for the hand-washing rotating chamber in the cases of without a hand and with a hand. In the first case, that is, without a hand inside the chamber, there are 132,643 nodes and 678,774 elements. The other case, which has one hand in the chamber, has 287,429 nodes and 1,158,678 elements in total. The maximum skewness of the mesh was 0.8373 and the maximum aspect ratio was 9.98. All of the surfaces, including of the human hand, are set as walls, and the inlets are located in the nozzles, which have a speed of 2–7 m/s. The orientation of this flow is perpendicular to the inlet.

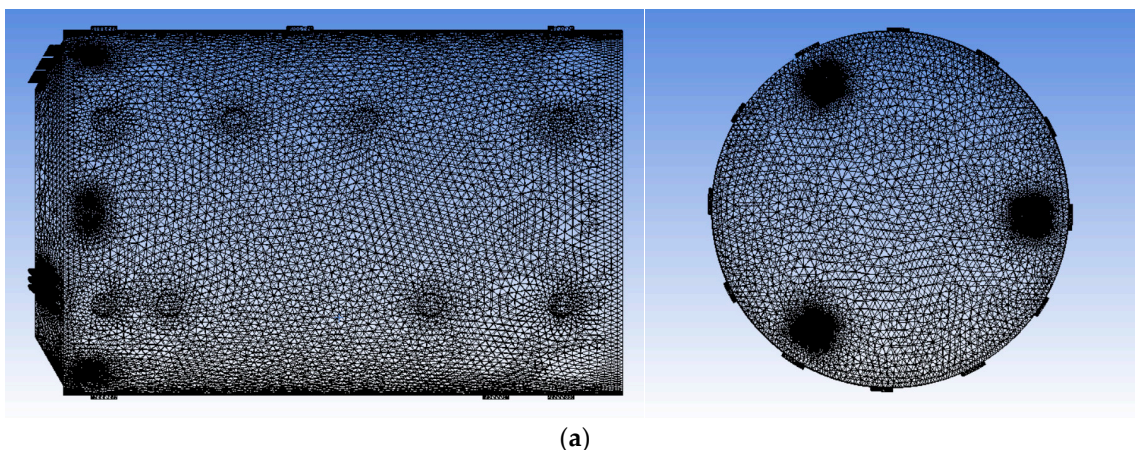


Figure 3. Cont.

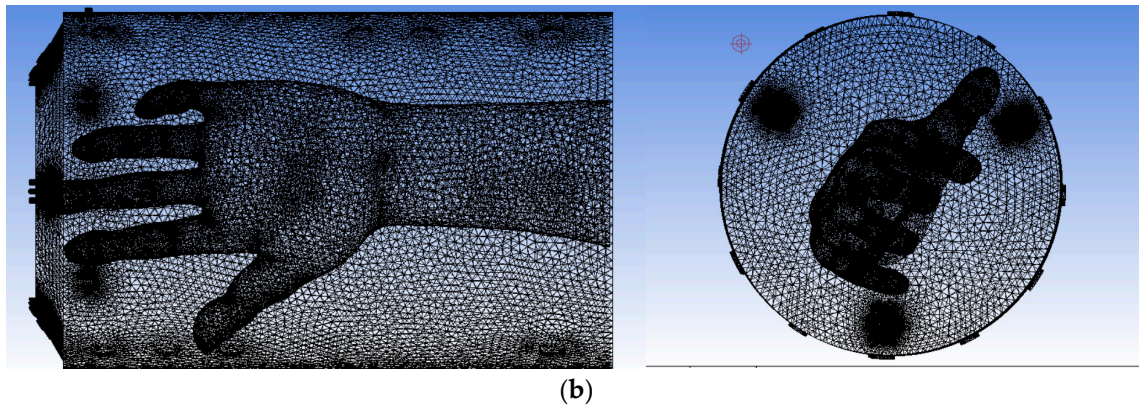


Figure 3. Typical mesh used in the computational domain for the hand-washing rotating chamber: (a) without a hand; (b) with a hand.

3. Results and Discussion

The results obtained from the simulations show that the flow is evenly spread throughout the chamber and around the human hand. Figure 4 illustrates the distribution of fluid flow through the entire rotating chamber at $t = 5$ s. Both pictures show the vector line of the liquid in the chamber being rotated by the mechanics of the machine; flows reach the bottom of the chamber and are strongly sprayed outside. A dense stream of the solution reaches the areas of the hands that can easily become infected with viruses. Specifically, the figure shows the distribution of the flow in the hand image, and it can be seen that in places where it is difficult to achieve a high degree of disinfection, such as the thumb and the gaps between the fingers, the density of the flow is still very good. Figure 5 shows the velocity at $t = 5$ s. The initial condition of the hand-washing chamber with a maximum speed (5 m/s) of liquid occurs at the nozzle, along with the rotational speed (40 rad/s) of the chamber. When water is sprayed, it forms streams of water with different vertical angles. Figure 5 also shows that the velocity of the water flow decreases nearer the middle of the chamber. This is entirely appropriate as there should be a hand-washing vortex in the middle of the chamber to remove the virus from the hands.

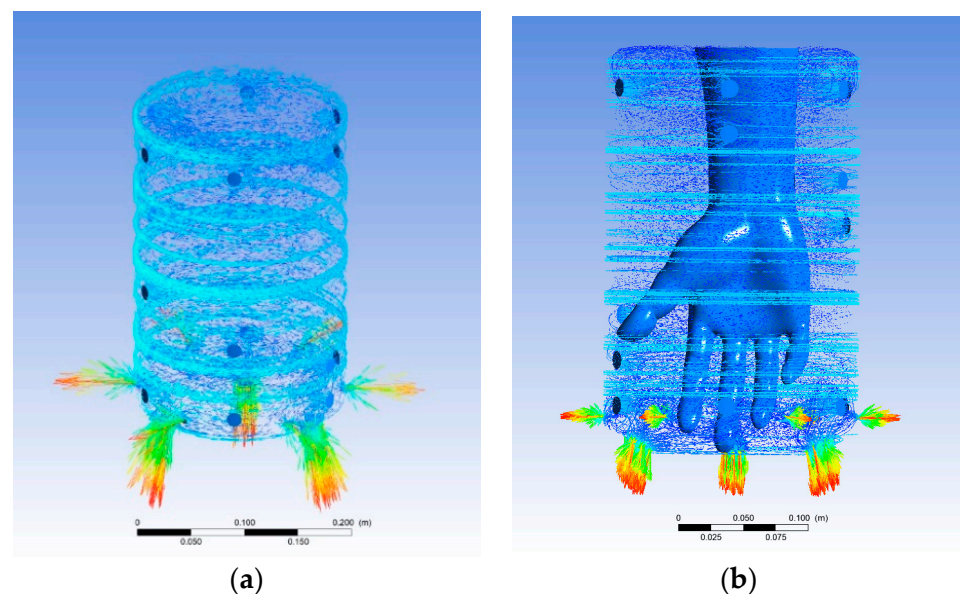


Figure 4. The flow distributions of the chamber: (a) without a human hand; (b) with a human hand.

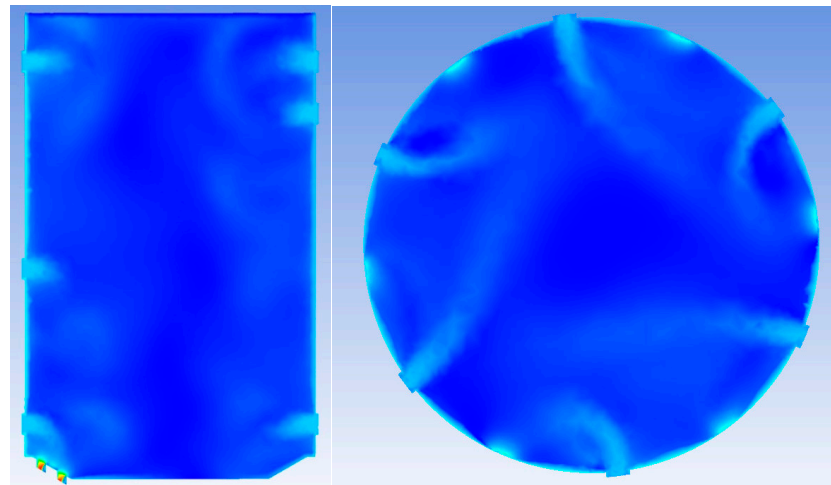


Figure 5. The velocity field of the chamber in the two cases.

Based on Figure 6, the distribution of the flow is appropriate as it covers all the space in the rotating chamber for the cases of without a hand and with a hand at $t = 5$ s. This information can be useful in subsequent optimizations of the design; it can be seen that, in the arm position, the flow density may be lower, whereas the hand needs a higher concentration of fluid density. In future, innovative solutions can be implemented to ensure that fluid dynamics retain an important role to enhance the effectiveness of cleaning.

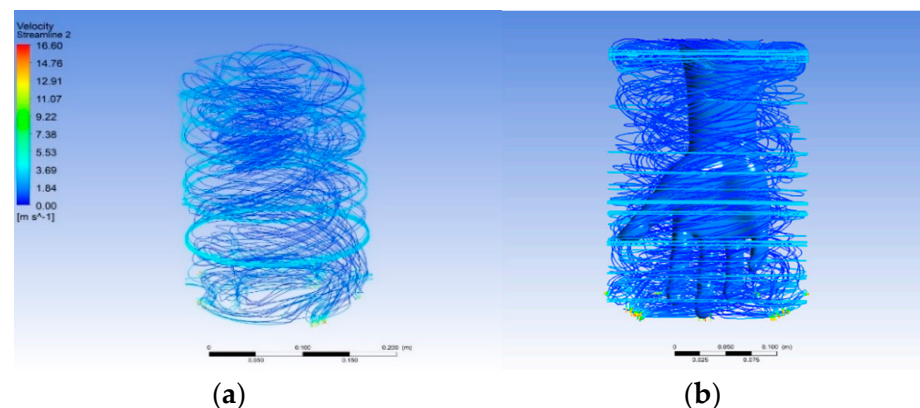


Figure 6. The streamlines of the chamber: (a) without a hand; (b) with a hand.

Figure 7a shows the flow distribution of the chamber at different times; the nozzles in turn spray a stream of hand-washing liquid. Based on the rotating mechanism of the hand-washing machine system, these hand-washing liquid lines will rotate at a speed of 40 rad/s. Here, the various times are considered to observe the change in hydrodynamic characteristics of the flow in the chamber when the hand-washing system operates. During this period, the vortices around the hands change significantly. Initially, the liquid is sprayed from the nozzles and the rotation speed of chamber is not reached (40 rad/s), so the liquid hits the chamber wall and bounces back to form whirlpools, which are created at different positions in the chamber by the liquid being partially held by centrifugal force on the walls of the chamber. In addition, when the liquid flows from the nozzle holes to the opposite wall, the liquid creates straight lines. Because there are no flow obstructions, the velocity of the liquid when entering the middle of the chamber is slightly reduced. Figure 7b shows the flow distribution of the liquid at different times. At $t = 1$ s, the liquid flows ejected by the nozzles produce the same phenomenon as in the case without a hand at the beginning. However, at this time, the hand is an obstacle that prevents the fluid from moving in a straight line. The flow of liquid moving to the hand creates many small

vortexes that are not very concentrated around the hand. At a later time, the vortexes are more concentrated around the hand.

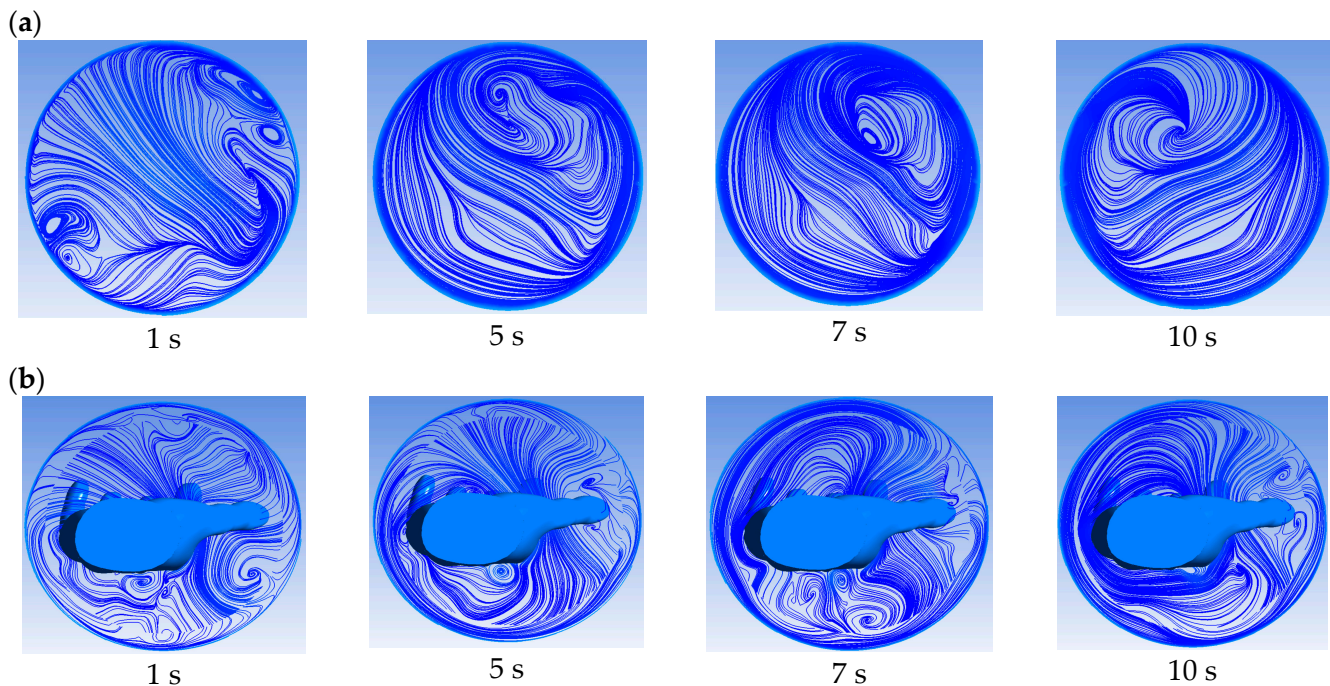


Figure 7. The flow distributions of the hand-washing chamber at different times for the two cases of (a) without a hand and (b) with a hand.

Figure 8 shows the mean velocity of fluid inside the hand-washing chamber in both the case without a hand and with a hand. The mean velocity of the liquid varies in a similar way during a hand-washing cycle of about 5 m/s. These values vary according to the curve resulting from the rotating mechanism of the hand-washing machine system, which rotates at a speed of 40 rad/s. In the case without a hand, the velocity has a relatively smooth up and down change because the draining holes are always opened with the fluid being continuously sprayed. The mean velocity through a point is lower than the initial velocity of the fluid because we chose to position the survey point in the middle of the chamber. In fact, the liquid flows sprayed into the hand-washing chamber also cause them to hit and reduce the velocity of the fluid. In the case with a hand in the hand-washing chamber, the velocity field has a shape quite similar to that in the case without a hand; however, when the fluid is sprayed against an obstacle (arm), the fluid is blocked. At a certain time, the velocity fluctuation in the liquid at the chosen point in the case with a hand is higher than that in the case without a hand in the hand-washing chamber. Therefore, when the fluid reaches the surface of the hand's skin, it creates low-pressure places near the hand and vortexes. This causes the velocity of the fluid to increase.

Figure 9 compares the pressure in the case without a hand and the case with a hand, with the rotation speed of chamber at 40 rad/s and the fluid speed at 5 m/s. In the beginning stage of both cases, the pressure rapidly increases to peak at the maximum value, and is then maintained at that level until the hand-washing procedure is completed. In the case with a hand in the chamber, the arm is an obstacle to the flow of the moving liquid; therefore, when the liquid comes into contact with the skin surface, the pressure in the case with a hand is higher than the pressure in the case without a hand.

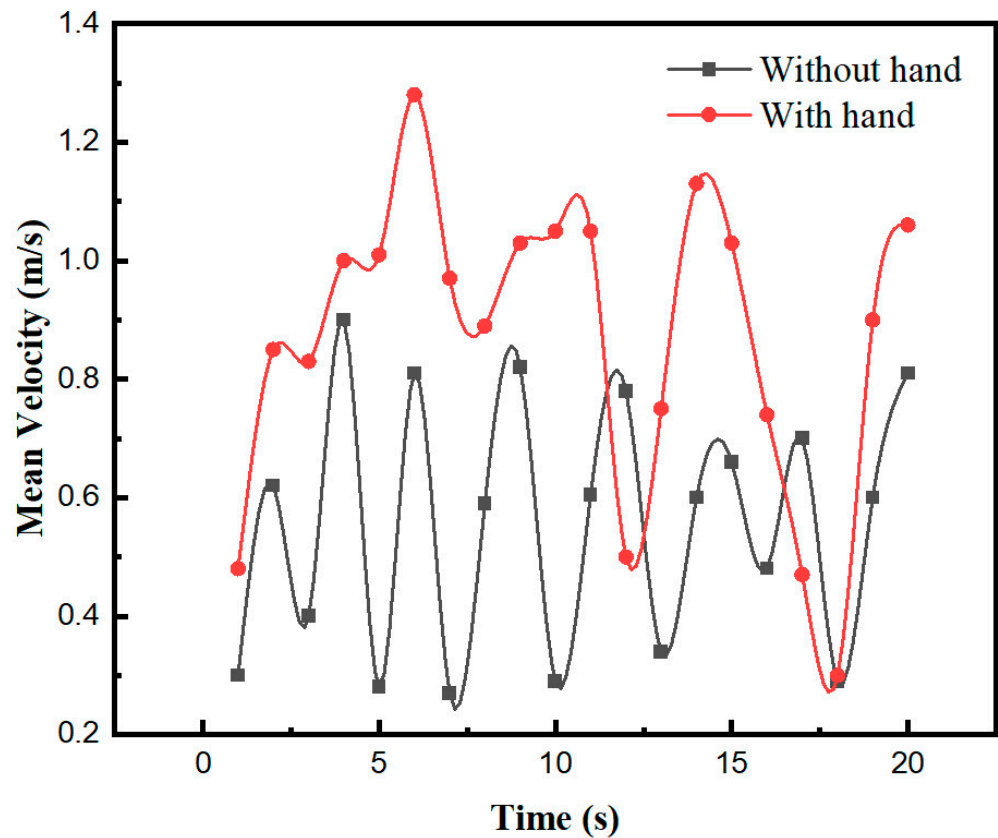


Figure 8. The mean velocity value inside the hand-washing chamber in the two cases without a hand and with a hand.

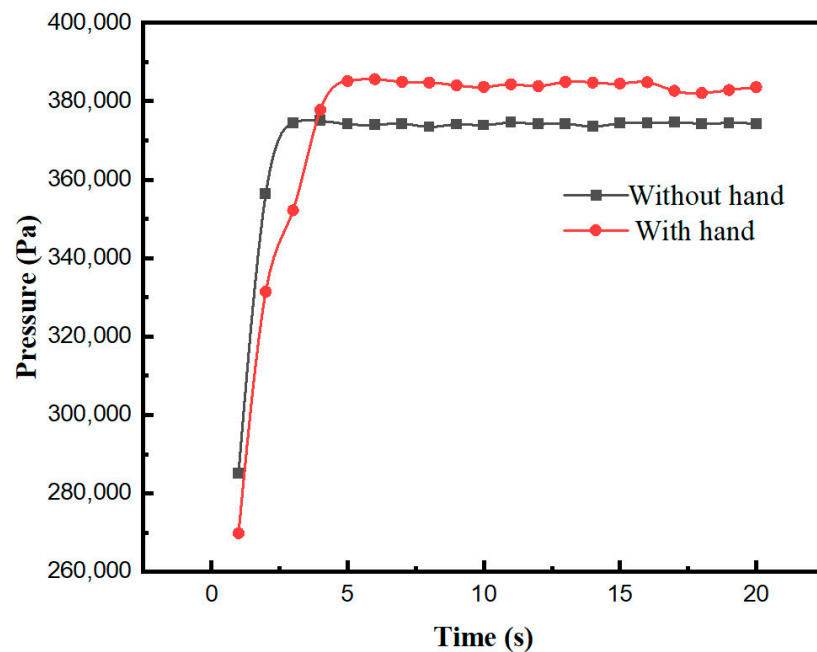


Figure 9. The pressure value inside the hand-washing chamber in the two cases of without a hand and with a hand.

Figure 10 illustrates the mean velocity through a point with rotation at a speed of 40 rad/s for the inlet flow rates of $Q = 462 \text{ mm}^3/\text{s}$, $770 \text{ mm}^3/\text{s}$, and $1078 \text{ mm}^3/\text{s}$. Figure 10a shows that, for the different inlet flow rates, the velocity through a point does not change much with the rise and fall in the fluid velocity in the hand-washing chamber. For the case

of $Q = 1078 \text{ mm}^3/\text{s}$, the average velocity is greater than that in the other two cases due to the change in the inlet flow. The velocity of the fluid that passes through the surveyed point increases because the drainage holes are not drained in time. If the water flow is too high, the fluid particles will be splashed out. In Figure 10b, we selected the point position for the model with the hand in the middle of the finger gap. In this case, the graph shows that there are times when the velocity changes are larger than in the case without a hand; at these times, large whirlpools are created to help remove bacteria. In particular, after the initial time, the hand-washing chamber starts to achieve the operating number of revolutions and the amplitude of the speed fluctuation is more pronounced, proving that the hand-washing chamber works effectively to clean hands.

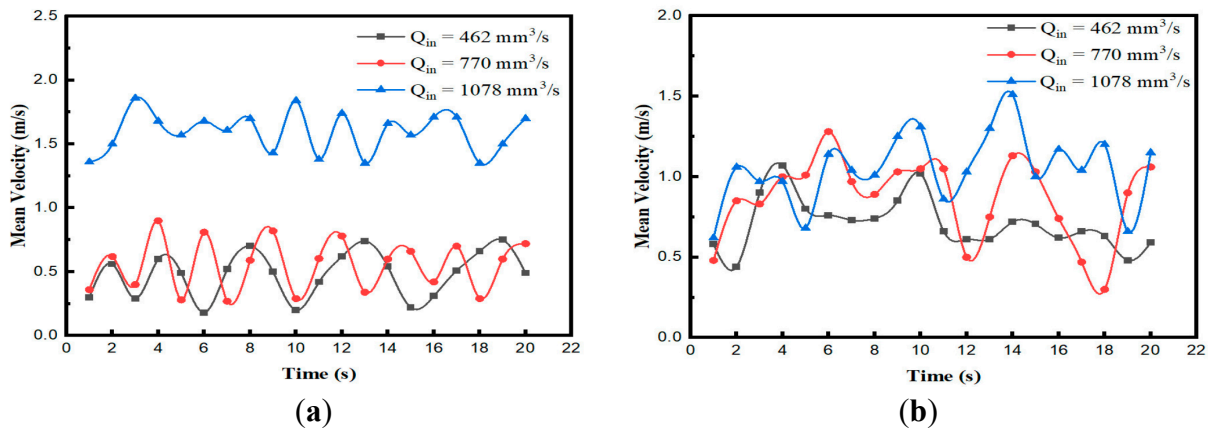


Figure 10. The mean velocity value inside the hand-washing chamber at different inlet flows in the cases of (a) without a hand and (b) with a hand.

Figure 11 shows the pressure in the two cases of the hand-washing chamber during a 20 s period. The pressure value in the chamber with a hand is larger than that in the chamber without a hand. Because the hand is an obstacle, the pressure at the survey point also increases at this time. Due to the reverse pressure created by the impact of the fluid jets on the hand, the machine takes about 2 s to reach the maximum pressure, which is maintained during the operation time. When the higher pressure is applied to the surface of the hand’s skin, it creates a larger force. This force contributes to helping to remove the bacteria attached to the skin’s surface.

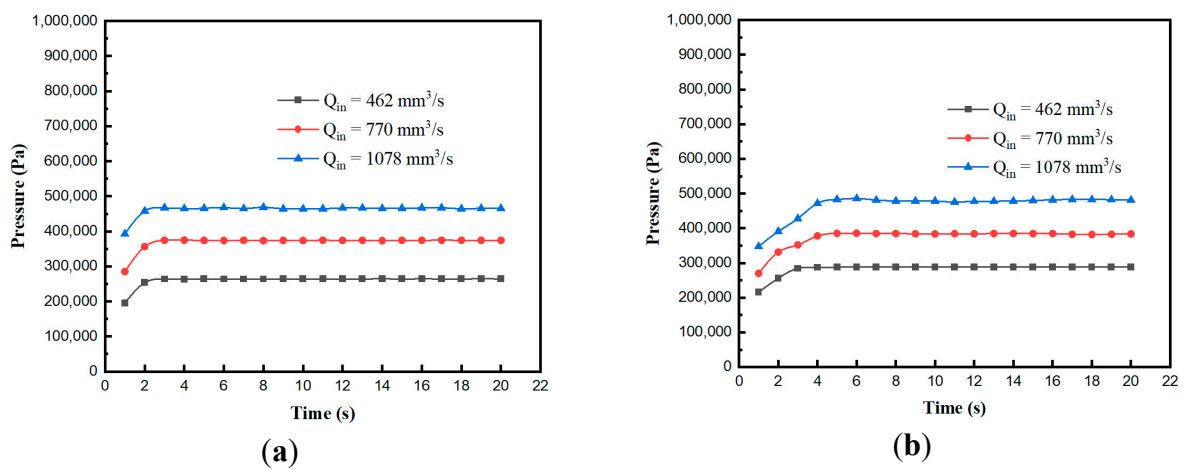


Figure 11. The pressure value inside the hand-washing chamber at different inlet flow rates in the cases of (a) without a hand and (b) with a hand.

4. Conclusions

In this study, a conceptual design of a hand-washing chamber was modeled, meshed, and analyzed to obtain characteristics such as pressure, velocity distribution, and flow. The initial velocity of the different nozzles, the liquid velocity, and the liquid pressure passing through a point change significantly. The combination of the velocity of the inlet holes with the mechanical rotation of the hand-washing chamber creates whirlpools that help to remove more bacteria.

The numerical results show that the higher the inlet flow rates, the larger the pressure in the hand-washing chamber. Once the pressure in the hand-washing chamber increases, bacteria are easily removed from the skin of the hands. The sterilization rate and bacteria drift increase when the inlet flow rates increase. This offers the potential idea to upgrade and optimize new designs having less energy usage and higher sterilization efficiency. The achievements presented in this paper can be used to implement innovative solutions.

The identification of a relationship between liquid inlet flow and increased pressure in the hand-washing chamber, and the high pressure, is useful to help eliminate pathogens. In the future, the results of the paper can also contribute to advancements in fluid dynamics and high-pressure water-jet nozzle technology.

Author Contributions: Conceptualization, T.-L.L. and T.-H.-N.V.; methodology, T.-L.L.; software, T.-H.P.; validation, T.-L.L., T.-H.-N.V. and T.-H.P.; formal analysis, T.-L.L.; investigation, T.-H.-N.V.; resources, T.-H.P.; data curation, T.-L.L. and T.-H.P.; writing—original draft preparation, T.-H.-N.V. and T.-H.P.; writing—review and editing, T.-L.L.; visualization, T.-H.P.; project administration, T.-L.L.; funding acquisition, T.-L.L. All authors have read and agreed to the published version of the manuscript.

Funding: This research received no external funding.

Data Availability Statement: The data presented in this study are available on request from the corresponding author.

Acknowledgments: We acknowledge the support of time and facilities from Ho Chi Minh City University of Technology (HCMUT), VNU-HCM for this study.

Conflicts of Interest: The authors declare no conflict of interest.

References

1. Wickramatillake, A.; Kurukularatne, C. SARS-CoV-2 human disinfection chamber: A critical analysis. *Occup. Med.* **2020**, *70*, 330–334. [[CrossRef](#)] [[PubMed](#)]
2. Riedel, S.; Edward, J.J. The History of Smallpox and Vaccination, Baylor University Medical Center Proceedings. *Med. Cent. Proc.* **2005**, *18*, 21–25.
3. Allegranzi, B.; Pittet, D. Role of Hand Hygiene in Healthcare-Associated Infection Prevention. *J. Hosp. Infect.* **2009**, *73*, 305–315. [[CrossRef](#)]
4. Conover, D.M.; Gibson, K.E. A Review of methods for the evaluation of handwashing efficacy. *Food Control* **2016**, *63*, 53–64. [[CrossRef](#)]
5. Kukkala, K.B.; Hough, C.; Jasinski, V.A.; Gill, N.; Alhouthi, N.; Ceballos, M. WashBot™ An Automatic Hand Washing Machine. *ASAIO J.* **2022**, *68*, 105. [[CrossRef](#)]
6. Jolan, B.S.; Marlon, G.R.; Eunelfa, R.C.; Alain, V.C.; Wubishet, D.; Assefa, S.Y. Multi-Station Automated Hand Washing System. *Int. J. Recent Technol. Eng.* **2020**, *9*, 36–43.
7. Le, T.-L.; Chen, J.-C.; Shen, B.-C.; Hwu, F.-S.; Nguyen, H.-B. Numerical investigation of the thermocapillary actuation behavior of a droplet in a microchannel. *Int. J. Heat Mass Transf.* **2015**, *83*, 721–730. [[CrossRef](#)]
8. Le, T.-L.; Chen, J.-C.; Hwu, F.-S.; Nguyen, H.-B. Numerical study of the migration of a silicone plug inside a capillary tube subjected to an unsteady wall temperature gradient. *Int. J. Heat Mass Transf.* **2016**, *97*, 439–449. [[CrossRef](#)]
9. Le, T.-L.; Chen, J.-C.; Nguyen, H.-B. Numerical study of the thermocapillary droplet migration in a microchannel under a blocking effect from the heated wall. *Appl. Therm. Eng.* **2017**, *122*, 820–830. [[CrossRef](#)]
10. Le, T.-L.; Chen, J.-C.; Nguyen, H.-B. Numerical investigation of the forward and backward thermocapillary motion of a water droplet in a microchannel by two periodically activated heat sources. *Numer. Heat Transf. Part A Appl.* **2021**, *79*, 146–162. [[CrossRef](#)]
11. Le, T.L.; Hong, T.D. Computational fluid dynamics study of the hydrodynamic characteristics of a torpedo-shaped underwater glider. *Fluids* **2021**, *6*, 252. [[CrossRef](#)]

12. Le, T.L.; Nghia, T.T.; Thong, H.D.; Son, M.H.K. Numerical study of aerodynamic performance and flow characteristics of a centrifugal blower. *Int. J. Intell. Unmanned Syst.* **2022**, *11*, 396–406. [[CrossRef](#)]
13. Tran, T.-H.; Le, T.-L.; Hong, D.-T.; Nguyen, T.-P. The effect of inlet velocities on the droplet size in T-junction microfluidic devices. *JP J. Heat Mass Transf.* **2022**, *28*, 1–14. [[CrossRef](#)]
14. Le, T.-L.; Nguyen, T.T.; Kieu, T.T. A CFD Study on the Design Optimization of Airborne Infection Isolation Room. *Math. Probl. Eng.* **2022**, *2022*, 5419671. [[CrossRef](#)]
15. Feurhuber, M.; Magno, M.; Miranda, M.; Prieler, R.; Hochenauer, C. CFD Investigation of Non-Condensable Gases in Vacuum and Non-Vacuum Steam Sterilizers. *Chem. Ing. Tech.* **2019**, *91*, 502–513. [[CrossRef](#)]
16. Lewinski, N.A.; Berthet, A.; Maurizi, L.; Eisenbeis, A.; Hopf, N.B. Effectiveness of Hand-Washing on the Removal of Iron Oxide Nanoparticles from Human Skin ex vivo. *J. Occup. Environmental Hyg.* **2017**, *14*, 115–117. [[CrossRef](#)] [[PubMed](#)]
17. Vuai, S.A.H.; Sahini, M.G.; Sule, K.S.; Ripanda, A.S.; Mwangi, H.M. A comparative in-vitro study on antimicrobial efficacy of on-market alcohol-based hand washing sanitizers towards combating microbes and its application in combating Covid-19 global outbreak. *Heliyon.* **2022**, *8*, 11689. [[CrossRef](#)]
18. Huang, L.Y.; Chen, Z.S. Effect of Technological Parameters on Hydrodynamic Performance of Ultra-High-Pressure Water-Jet nozzle. *Appl. Ocean Res.* **2022**, *129*, 103410. [[CrossRef](#)]
19. Shih, T.-H.; Liou, W.W.; Shabbir, A.; Yang, Z.; Zhu, J. A new $k-\epsilon$ eddy viscosity model for high Reynolds number turbulent flows. *Comput. Fluids* **1995**, *24*, 227–238. [[CrossRef](#)]
20. Jin, Y.; Liu, C.-L.; Song, X.-F.; Yu, J.-G. Computational fluid dynamics simulation as a tool for optimizing the hydrodynamic performance of membrane bioreactors. *RSC Adv.* **2019**, *9*, 32034–32046. [[CrossRef](#)]
21. Feurhuber, M.; Cattide, A.; Magno, M.; Miranda, M.; Prieler, R.; Hochenauer, C. Prediction of the fluid flow, heat transfer and inactivation of microorganism at medical devices in modern steam sterilizers using computational fluid dynamics. *Appl. Therm. Eng.* **2017**, *127*, 1391–1403. [[CrossRef](#)]
22. Feurhuber, M.; Magno, M.; Miranda, M.; Hochenauer, C. CFD investigations of steam penetration, air-removal and condensation inside hollow loads and cavities. *Appl. Therm. Eng.* **2019**, *147*, 1070–1082. [[CrossRef](#)]
23. Brauer, M.; Zhao, J.T.; Bennitt, F.B.; Stanaway, D. Global Access to Handwashing: Implications for Covid-19 control in Low-income Countries. *Environ. Health Perspect.* **2020**, *128*, 069001. [[CrossRef](#)] [[PubMed](#)]
24. Phillips, A.B.; Turnock, S.R.; Furlong, M. The Use of Computational Fluid Dynamics to Aid Cost-Effective Hydrodynamic Design of Autonomous Underwater Vehicles. *Proc. Inst. Mech. Eng. Part M J. Eng. Marit. Environ.* **2010**, *224*, 239–254. [[CrossRef](#)]

Disclaimer/Publisher’s Note: The statements, opinions and data contained in all publications are solely those of the individual author(s) and contributor(s) and not of MDPI and/or the editor(s). MDPI and/or the editor(s) disclaim responsibility for any injury to people or property resulting from any ideas, methods, instructions or products referred to in the content.